Conformational Dynamics of M2 Helices in KirBac Channels: Helix Flexibility in Relation to Gating via Molecular Dynamics Simulations†

Alessandro Grottesi,‡,|| Carmen Domene,§,|| Benjamin Hall,‡ and Mark S. P. Sansom*,‡

Department of Biochemistry, University of Oxford, South Parks Road, Oxford, OX1 3QU, U.K., and Physical and Theoretical Chemistry Laboratory, Department of Chemistry, University of Oxford, South Parks Road, Oxford, OX1 3QZ, U.K.

Received June 2, 2005; Revised Manuscript Received August 31, 2005

ABSTRACT: KirBac1.1 and 3.1 are bacterial homologues of mammalian inward rectifier K channels. We have performed extended molecular dynamics simulations (five simulations, each of >20 ns duration) of the transmembrane domain of KirBac in two membrane environments, a palmitoyl oleoyl phosphatidylcholine bilayer and an octane slab. Analysis of these simulations has focused on the conformational dynamics of the pore-lining M2 helices, which form the cytoplasmic hydrophobic gate of the channel. Principal components analysis reveals bending of M2, with a molecular hinge at the conserved glycine (Gly134 in KirBac1.1, Gly120 in KirBac3.1). More detailed analysis reveals a dimer-of-dimers type motion. The first two eigenvectors describing the motions of M2 correspond to helix kink and swivel motions. The conformational flexibility of M2 seen in these simulations correlates with differences in M2 conformation between that seen in the X-ray structures of closed channels (KcsA and KirBac) in which the helix is undistorted, and in open channels (e.g. MthK) in which the M2 helix is kinked. Thus, the simulations, albeit on a time scale substantially shorter than that required for channel gating, suggest a gating model in which the intrinsic flexibility of M2 about a molecular hinge is coupled to conformational transitions of an intracellular 'gatekeeper' domain, the latter changing conformation in response to ligand binding.

Potassium (K) channels (*1*) provide an opportunity to explore the relationship between membrane protein structure, dynamics, and function. K channels are of physiological and biomedical interest. They regulate K^+ ion flux across cell membranes. K channel regulation is accomplished by a conformational change that allows the protein to switch between two alternative (closed vs open) conformations, a process known as gating. Gating is thus an inherently dynamic process that cannot be fully characterized by static structures alone.

The elucidation of the structures of several K channels (*2*) has shed considerable light on the structural basis of the mechanisms of ion selectivity and permeation (*3*−*10*). All of these structures (for KcsA, gated by low pH; for MthK, gated by Ca^{2+} ions; for KvAP and Kv1.2, gated by transmembrane voltage; for KirBac, gating mechanism unknown) share a tetrameric pore-forming domain, in which the monomers surround a central pore. Each subunit contains an M1-P-F-M2 motif (or S5-P-F-S6 in Kv channels), where M1 and M2 are transmembrane helices, and the short P-helix and extended filter (F) region form a re-entrant loop between the two TM helices.

Inward rectifier (Kir) channels have a relatively simple TM architecture, containing only the M1-P-F-M2 motif (in contrast with e.g. the voltage gated Kv channels which contain four additional helices associated with voltage-sensing). In humans, Kir chanels have two main physiological roles: they regulate cell excitability by stabilizing the membrane potential close to the K-equilibrium potential, and they are involved in K-transport across membranes (*11*, *12*). Recent structures, of the intracellular domain of mammalian Kir (GIRK1; (*13*)) and of the complete channel (i.e. TM and intracellular domains) of two bacterial Kir homologues (KirBac1.1 at 3.7 Å resolution (*9*) and KirBac3.1 at 2.6 Å resolution (*14*)), provide an opportunity to obtain a detailed understanding of structure/function relationships in this important family of K channels.

KirBac1.1 is the first bacterial Kir whose structure has been solved (*9*). The overall TM topology is similar to that of the simple bacterial channel KcsA, with the addition of a 'slide' helix N-terminal to the M1 TM helix. KirBac1.1 also has an intracellular (IC) domain consisting mostly of β-sheet, with a fold related to that of the GIRK1 IC domain. The KirBac1.1 channel is in a closed (i.e. nonconducting) conformation, as the intracellular pore mouth, formed by the crossing point of the C-termini of the M2 helices, is hydrophobic and very narrow (only ∼0.05 nm in radius, compared with the 0.133 nm radius of a K^+ ion). KirBac3.1 has the same overall architecture as KirBac1.1 (and indeed the two channels share 40% sequence identity). However, KirBac3.1 seems to have been captured in what is suggested to be an intermediate (although still largely closed) state in its crystal structure (*14*), with a pore radius at the intracellular mouth of 0.12 nm. The selectivity filters of both KirBac

† This work was supported by a grant from the Wellcome Trust. C.D. is a Royal Society University Research fellow.

* To whom correspondence should be addressed. E-mail: mark@biop.ox.ac.uk. Phone: +44-1865-275371. Fax: +44-1865-275182.

‡ Department of Biochemistry.

§ Department of Chemistry.

|| These two authors contributed equally to this work.

10.1021/bi0510429 CCC: $30.25
Published on Web 10/14/2005

Table 1: Summary of Simulations[a]

simulation	membrane	number of octanes or POPCs	total number of atoms	K^+ ions	Cα RMSD[b] (nm) all residues	Cα RMSD[b] (nm) TM helix residues	Cα RMSD[b] (nm) M2 helix residues
KirBac1.1							
OCT1	octane	662	51324	S1 and S3	0.55	0.17	0.13
OCT2	octane	662	51321	S_{EXT} and S2	0.56	0.17	0.12
PC1	POPC	208	54969	S1 and S3	0.33	0.15	0.15
PC2	POPC	208	54979	S2	0.22	0.13	0.14
KirBac3.1							
PC3	POPC	196	68964	S_{EXT}, S0, S1, and S4	0.23	0.15	0.09

[a] All simulations were of ≥20 ns duration. [b] The Cα RMSD from the initial conformation was averaged over the final ≥18 ns of each simulation, i.e., discarding the first 2 ns of the simulation. The TM helix residues of KirBac1.1 are defined as M1 (60−82), P (97−109), and M2 (120−150). The corresponding residues for KirBac3.1 are M1 (46−71), P (82−95), and M2 (106−136).

channels are very similar to that of KcsA, with a succession of five potential K^+ ion binding sites formed by cages of eight oxygen atoms.

Channel activation is achieved by a conformational change from a closed to an open state. This process is known as gating (*15*). We may consider this process in terms of two regions of the channel. The gate per se is the structural element that prevents ion flow when the channel is in a closed state, whereas a sensor or 'gatekeeper' domain couples the conformational state of the gate to changes in the cellular environment of the channel. Thus, in voltage-gated K channels the S1−S4 helix domain acts as a voltage sensor, coupled to conformational changes in the pore-lining S6 helix (*1*, *2*, *8*, *16*). In Kir channels it is thought that the IC domain acts as a 'gatekeeper', interacting with various possible ligands (*13*, *17*−*19*) to regulate the conformational state of the TM domain gate.

There is considerable structural (*6*, *7*), functional (*16*, *20*, *21*), and computational (*22*, *23*) evidence suggesting that gating per se of K channels is associated with a change in conformation of the pore-lining M2 (or in Kv channels S6) helices. Thus, comparison of the structure of the closed state of KcsA and of the open state of MthK reveals that in the latter the pore-lining M2 helices are bent in the vicinity of a conserved glycine residue to open up the hydrophobic gate at the intracellular mouth of the pore (*7*, *24*). It has been suggested that this model is applicable to all K channels. If so, then the M2 helices should exhibit an intrinsic flexibility in other K channels, such as KirBac.

Computational approaches, based on molecular dynamics (MD) simulations of K channels, provide an approach to exploring conformational flexibility of such proteins in relation to their biological function (*25*−*48*). For example, a number of studies have discussed the role played by flexibility of the selectivity filter and how this might affect ion permeation (e.g. *47*, *49*−*51*). These indicate that the static picture of a K^+ ion that fits exactly within the cage of oxygens in the filter does not properly describe permeation of ions through the filter. A number of studies, using e.g. normal modes analysis (*22*), molecular modeling (*24*, *52*, *53*), and nonequilibrium MD simulations (*23*), have described how K channel gating may be achieved by outward motion of the pore-lining M2 helices. Here we describe the use of molecular dynamics (MD) simulations of the TM domain to explore the short (∼10 ns) time scale conformational dynamics of the M2 helices in KirBac1.1 and KirBac3.1. Our purpose is to investigate the role played by flexibility in the local conformational dynamics of the gate region. Such simulations provide clues as to the nature of longer time scale (∼0.1 ms) gating conformational changes in Kir channels.

METHODS

We have simulated the transmembrane domain of KirBac1.1 in two different membrane-mimicking environments (an octane slab and a POPC bilayer; Table 1) and that of KirBac3.1 in a bilayer environment. The KirBac1.1 simulations were extensions (from 10 ns to >20 ns) of those described previously (*51*). The initial protein coordinates were taken from PDB (www.rcsb.org) entries 1P7B (for KirBac1.1) and 1XL4 (for KirBac3.1). The transmembrane domain was defined as extending from residue 40 to 153 in KirBac1.1 and from residue 30 to 138 in KirBac3.1. There was a shared proton between Glu106 and Asp115 of KirBac1.1, homologous to that shared between Asp80 and Glu71 in KcsA (*54*). The rest of the residues remained in their default ionization state. The system (i.e. protein plus membrane) were solvated with SPC water molecules (*55*) retaining all the crystallographic waters. A water molecule was placed at the "back" of the selectivity filter of KirBac1.1, between the pair Glu106-Asp115 to mimic the equivalent water in KcsA. Indeed, the buried location and relative orientation position of the side chains of Glu106 and Asp115 is very was similar to that in KcsA, suggesting a degree of conservation across the potassium channel family. In KirBac3.1 the corresponding waters behind the selectivity filter were taken from the crystal structure. An ionic strength of 150 mM was used, with counterions added where needed to keep all systems electrically neutral.

Simulations were performed using minor modifications of methods described previously (*43*, *56*). For the simulations in a lipid bilayer, the protein was positioned in a preequilibrated 1-palmitoyl-2-oleoyl-phosphatidyl choline (POPC) bilayer so as to maximize possible interaction of the POPC headgroups and the 'belts' (see below) of amphipathic aromatic side chains on the protein surface. For the membrane-mimetic octane slab simulations, a slab of thickness 3.2 nm was used. Once the protein was inserted in the bilayer or surrounded by octane, an equilibration was performed during which the protein atoms were restrained for 0.2 ns. The restraints were then removed and production simulations of 10 ns of duration followed.

MD simulations were performed with GROMACS 3.1.4 (*57*) (www.gromacs.org) with a modified version of the GROMOS-87 force field (*58*). Lipid parameters were based on those described in refs 59 and 60. The lipid−protein

interactions used GROMOS parameters. Parameters derived from those described in 61 were used for the K^+ ions. Simulations were carried out in the NPT ensemble, with periodic boundary conditions. The initial velocities were taken randomly from a Maxwellian distribution at 300 K. The temperature was held constant by coupling to an external bath (*62*). Long-range electrostatic interactions were calculated using the Particle Mesh Ewald summation methods (*63*). Lennard−Jones interactions were calculated using a cutoff of 0.9 nm. The pair lists were updated every 10 steps. The LINCS algorithm (*64*) was used to constrain bond lengths. The time step was 2 fs, and coordinates were saved every 0.1 ps.

Simulations were analyzed by means of principal component analysis (*65*): trajectories were projected along selected eigenvectors to filter the relevant motions (*66*). The program SWINK has been used to measure the swivel and kink angles of the helices (*67*). Molecular visualization and structural diagrams used VMD (*68*) and Rasmol (*69*). Convergence analysis of the principal components was performed according to refs 70 and 71. Briefly, to measure the convergence of the essential degrees of freedom, the normalized overlap between the first 10 eigenvectors of the positional fluctuation covariance matrix was calculated using trajectories sampled on five different time windows (the largest being 10 ns).

Anisotropic network models were generated using a modified version of the ANM code from the Jernigan laboratory (http://ribosome.bb.iastate.edu/) (*72*, *73*). A cutoff of 7 Å was used, above which distance no springs were defined, and below which all springs were defined as having equal forces. An (arbitrary) spring constant of 1 was used.

RESULTS

Simulation Systems. Before discussing the results it is helpful to discuss the design of the simulations (Table 1). For all simulations just the TM domain of KirBac was employed. This was because we wished to look at the intrinsic flexibility of the M2 helices, which are located in the TM domain, in the hope that this might provide some clues as to the nature of the motions underlying the early stages of gating in the intact channel. Of course, we cannot hope to address directly the process of gating (whose estimated time scale is ∼0.1 ms) by atomistic MD simulations. However, by releasing the TM domain from the control of the 'gatekeeper' IC domain, we hoped we might unmask at least some of the intrinsic gating-related motions of the TM domain. To further enhance such motions, we performed simulations in two environments: a lipid bilayer and an octane slab. Previous studies (*43*, *74*) have suggested that the latter, which has a lower viscosity than a lipid bilayer, might result in some degree of enhancement of the TM domain mobility, although comparison with the bilayer simulations is necessary to guard against artifacts. For each environment we performed two simulations for KirBac1.1, starting with different configurations of K^+ ions and water molecules within the selectivity filters of the channel (see ref 51 for details). In addition to the KirBac1.1 simulations, which are based on a relatively low resolution (3.7 Å) starting structure, we have also performed a simulation (PC3; see Table 1) of KirBac3.1 (resolution 2.6 Å) in a lipid bilayer. This enables us to examine whether the conformational dynamics of KirBac1.1 are conserved for other proteins of the same channel family. This approach, using comparative MD simulations to test the generality of observed motions, has already proved valuable for other (nonmembrane) proteins (see e.g. refs 75 and 76).

Protein Stability and Simulation Convergence. The first thing we addressed in this study is the degree of conformational drift from the initial structure of the TM domain and also the degree of subsequent convergence of the systems simulated. To measure conformational drift, we have analyzed the root-mean-square deviation (RMSD) of the Cα atoms from starting structure for the various TM α-helices. The results of this analysis (see Table 1) confirm that the overall degree of conformational drift is greater for the OCT than for the PC simulations. However, closer inspection reveals that the difference is somewhat less if one considers just the TM helices. Thus, the OCT environment may enable somewhat greater conformational flexibility in the TM domain than does the PC domain (on a ∼20 ns time scale) but does not result in an unacceptable degree of distortion of the TM domain, as reflected by the relatively low (0.15 nm) Cα RMSDs. Comparison of simulations PC1, PC2, and PC3 suggest that the conformational drift magnitudes are similar for KirBac1.1 and KirBac3.1, at least within a PC bilayer on a ∼20 ns time scale. Thus, the lower resolution of the KirBac1.1 structure does not seem to have resulted in a significantly greater extent of conformational drift.

A more quantitative comparison of protein mobility in the different simulations was carried out by means of block analysis of the mean square fluctuations (MSFs) of Cα atoms (*77*, *78*). For the last 20 ns of each simulation, MSF averages were calculated for time windows ranging from ∼0.1 to ∼10 ns and plotted as log−log graphs (see Supporting Information). From the nonzero slopes of the lines we concluded that the time-averaged MSF had not converged in any of the simulations. This is a general property of the current time scales (tens of nanoseconds) accessible by MD simulations of protein systems (*78*). However, we can still analyze trends in relative magnitudes of MSFs. This analysis suggests that for smaller time windows (<5 ns) the fluctuations of the M2 helix bundle in the OCT simulations are ∼1.4× greater than those in the corresponding PC simulations, with slower convergence of the latter such that the OCT and PC MSFs only become approximately equal for the ∼10 ns windows.

Principal Components Analysis. Principal components analysis (PCA) allows the motions of a protein to be decomposed down into their principal components (*65*, *66*). By performing such analysis on the backbone atoms of the pore-lining M2 helices in each simulation, it is possible to focus on the conformational fluctuations in these helices that might be expected to be related to gating of the pore, as in the crystal structure it is the extended M2 helices that bring together the Phe-146 side chains to form the hydrophobic gate (see Figure 1B). The results of this analysis yield eigenvectors describing the principal motions of the M2 helices, and the corresponding eigenvalues which provide the relative weights of each component to the total helix fluctuation. Note that we do not expect ∼20 ns simulations of the TM domain to reveal gating per se but rather to reveal the intrinsic flexibility of the pore-lining elements that may be exploited in the overall channel gating mechanism.

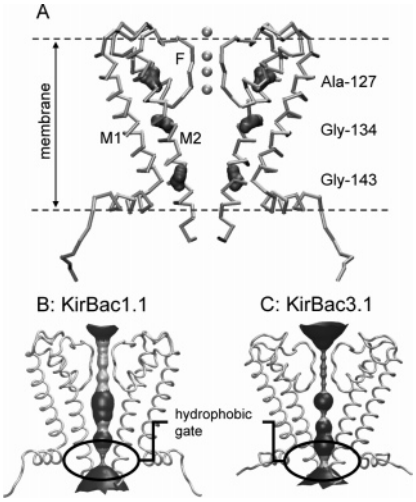

FIGURE 1: A. Schematic representation of the transmembrane domain of KirBac1.1, showing two of the four subunits. The locations of the filter (F) and of TM helices M1 and M2 are shown. Residues Ala-127, Gly-134, and Gly-143 are shown is space fill format. The horizontal broken lines indicate the approximate extent of the membrane (octane or POPC) used in the simulations. B. Pore lining surface (calculated using HOLE (*98*)) for the crystal structure of KirBac1.1 showing the region of the hydrophobic gate formed by the ring of Phe-146 side chains (radius ~0.05 nm). C. Pore lining surface for the crystal structure of KirBac3.1 (PDB code 1XL4) showing the region of the hydrophobic gate formed by the ring of Tyr-132 side chains (radius ~0.12 nm).

We also performed a convergence analysis (as described in refs 70 and 71; see Methods) of the motions of the Cα atoms of the M2 helices. This was intended to measure the extent to which the conformational space of the M2 (i.e. inner) helix bundle of our system was sampled during the simulations. The results indicate that, on a few tens of nanoseconds time scale, the normalized overlap of the essential motions converges to a value of ~0.6. For protein simulations, this represents a typical degree of overlap for the essential spaces as indicated by simulations studies of various proteins (*79*, *80*).

On average for the four subunits, the cumulative fluctuation in helix M2 given by the first two eigenvector components ranged from ~30% (for simulation OCT1) to ~73% (simulation PC2). The corresponding figure for simulation PC3 is ~40%. Therefore, in our subsequent analysis we will focus on the first two eigenvectors for each simulation.

The structural implications of this analysis may be visualized by calculating a set of snapshots in Cartesian space from the projection of frames of the simulation trajectories onto the corresponding eigenvectors. A schematic representation of the motion from the displacements along eigenvector 2 (for simulation OCT2, subunit 1) is shown in Figure 2. We have represented the motion in two fashions: first by fitting (i.e. superimposing) all Cα atoms of the M2 helix, and second by fitting just the Cα atoms of those residues N-terminal to the proposed Gly-134 hinge (i.e. residues 121−134). The first representation (Figure 2A) shows the overall flexibility of M2, both at the termini and in the vicinity of Gly-134; the second representation (Figure 2B) emphasizes the behavior of Gly-134 as a molecular hinge. Also shown (Figure 2C) is a schematic representation of how motions about a molecular hinge in a TM helix may be analyzed in

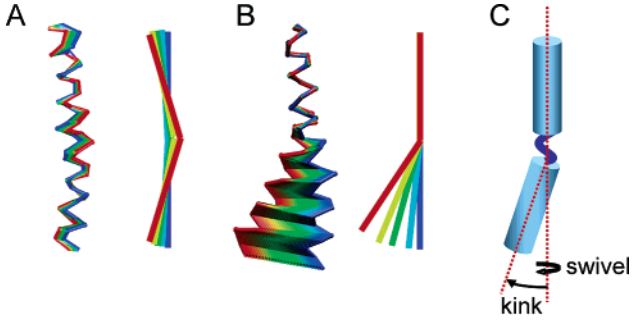

FIGURE 2: M2 helix motions from PCA. Snapshots of an M2 helix from simulation OCT2 are shown for eigenvector 2 (for which the dominant motion was helix kinking). In A, the snapshots are fitted on all residues; in B, the fitting is just on the residues of the N-terminal half of the helix (residues 121−134). The colors show 25 snapshots taken at equally spaced projections along the 2nd eigenvector. To the right of each Cα trace superimposition is a schematic representation of the equivalent superimposition of the (kinked) helix axes. C illustrates the definition of kink and swivel angle used elsewhere in this paper.

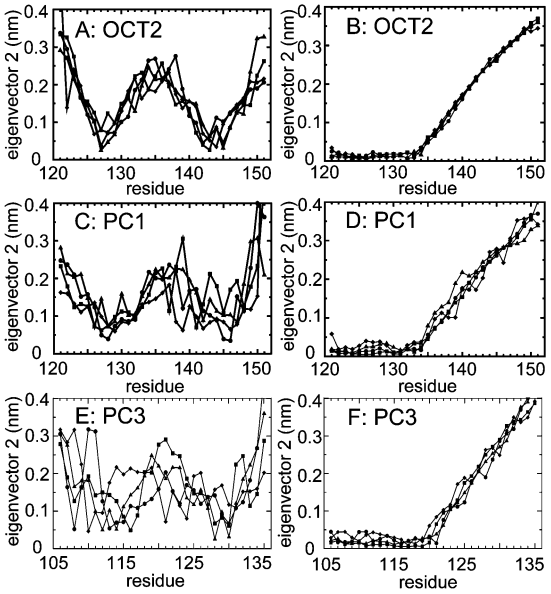

FIGURE 3: PCA analysis of M2 helix motions. Mean square displacements of the Cα atoms according to eigenvector 2 for: A,B, KirBac1.1, simulation OCT2; C,D, KirBac1.1, simulation PC1; and E,F, KirBac3.1, simulation PC3. For A,C,E, all M2 Cα atoms are used for the fitting prior to RMSD calculation; for B,D,F, the fitting of the helices uses only the Cα atoms of the N-terminal half (residues 121−134 for KirBac1.1, residues 106−120 for KirBac3.1) of M2

terms of a kink and swivel angle. This has proved useful in previous analyses of molecular hinges due to proline residues (*67*, *81*). It is evident that the eigenvector 2 motion shown in Figure 2A,B corresponds largely to a kink motion. We will return to this classification of molecular hinge motions in more detail below.

The same motions may be analyzed more quantitatively by plotting the mean square displacement (MSD) along the second eigenvector of all four M2 helices for simulations OCT2, PC1, and PC3 (Figure 3). Once again, the results may be shown either for fitting on all Cα atoms of M2 (Figure 3A,C,E) or just the Cα atoms of the N-terminal half (Figure 3B,D,F). Both analyses clearly confirm that there is a molecular hinge in the vicinity of residue 134 (in KirBac1.1) or its equivalent (residue 120) in KirBac3.1. For

Table 2: M2 Helix Kink and Swivel Angles

simulation	mean kink angle ± SD (deg)[a]	mean swivel angle ± SD (deg)[a]
KirBac1.1		
X-ray	12.5, 12.0, 12.5, 12.0	138, 140, 138, 140
OCT1	13.7 ±6.7, 19.9± 7.9, 12.7 ± 7.5, 13.0 ± 6.6	189 ± 50, 172 ± 26, 150 ± 102, 147 ± 65
OCT2	15.7 ± 7.3, 15.0± 7.1, 17.0 ± 7.9, 11.9 ± 5.8	149 ± 49, 216 ± 50, 159 ± 39, 184 ± 73
PC1	12.1 ± 6.4, 15.4± 6.8, 18.0 ± 7.6, 10.2 ± 5.6	207 ± 74, 137 ± 49, 188 ± 37, 154 ± 97
PC2	9.0 ± 4.6, 8.6± 4.4, 8.5 ± 4.4, 23.0 ± 6.9	183 ± 59, 187 ± 61, 140 ± 70, 188 ± 13
KirBac3.1		
X-ray	9.8, 5.2, 10.7, 5.4	228, 244, 236, 242
PC3	22.0 ± 8.9, 20.3± 7.9, 15.4 ± 7.0, 10.9 ± 5.9	261 ± 53, 222 ± 28, 221 ± 48, 192 ± 80

[a] The M2 helix kink and swivel angles (see Figure 3C for definition) are shown for the four KirBac helices. Values were averaged after discarding the first 2 ns of each simulation, and were calculated using Gly-134 (or Gly-120 for KirBac3.1) as a hinge point.

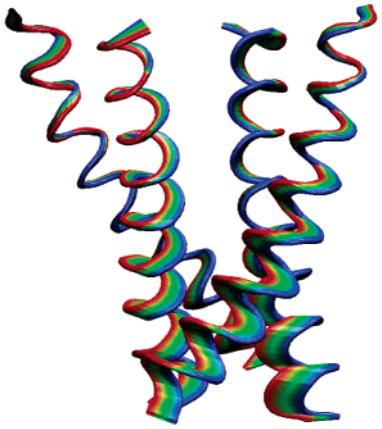

FIGURE 4: Snapshots of the M2 helix bundle corresponding to projections along the second eigenvector for the KirBac1.1 OCT2 simulation. The colors correspond to 25 Cα trace structures fitted on residues 121−134.

each simulation, the same pattern is seen for all four helices of the KirBac channel. The overall pattern is clearer for the OCT2 than for the PC1 and PC3 simulations: this is presumed to reflect more complete conformational sampling in the lower viscosity octane slab than in the POPC membrane. However, it is evident that the overall pattern is the same in both simulation environments. (The origin of the two patterns depending on which residues are used for fitting may be seen from the schematic helix axis diagrams in Figure 2).

One may explore the consequences of the hinge bending motion of the M2 helices for the channel as a whole by visualizing the displacement of all four helices along their corresponding second principal component (Figure 4). Clearly, all four KirBac1.1 monomers show the same distinct pattern of bending around Gly-134. This results in maximum perturbation of the bundle in the region of the hydrophobic gate formed by Phe-146.

Significantly, the hinge residue Gly-134 (Gly-120 in KirBac3.1) corresponds to a conserved residue within the K channel family. Comparison of crystal structures of a closed K channel (KcsA) and an open K channel (MthK) has been used to suggest that this conserved glycine may serve as a molecular hinge (*6*, *7*). Our analysis of the dynamics of M2 helix flexibility in KirBac confirms this suggestion.

Swivel and Kink Analysis. We may extend the PCA analysis to ask whether the motion about a glycine hinge may be decomposed into a helix kink and helix swivel term. Such analysis has already proved valuable for characterizing proline-induced distortions of TM helices (*67*). Given that proline may play a role in the gating of Kv channels (where the S6 helix, homologous to M2 of Kir channels, contains a conserved PVP motif) (*16*, *20*, *82*, *83*), it is of some interest to discover whether a glycine-hinge can enable similar kink and swivel motions.

First, let us note the kink and swivel angles in the crystal structure of KirBac (Table 2). The values for monomers 1 and 3 are the same and slightly different from those of monomers 2 and 4. This is a consequence of the degree of 2-fold symmetry (i.e. dimer of dimers) present in the KirBac crystal structure (*9*). However, the deviation from exact 4-fold symmetry in the TM domain is only very small in the X-ray structure.

Next, we can measure the mean kink and swivel angles in all six simulations (Table 2). Two interesting trends emerge. First, e.g. the mean M2 helix kink angles are a little higher in the octane than in the POPC simulations, reflecting the more complete sampling of M2 motions in the less viscous octane environment. Second, if for any one simulation one compares the four mean swivel angles for the four M2 helices, the dimer-of-dimers pattern is preserved (i.e. high-low-high-low for swivel angles). Thus it appears that the M2 bundle may behave dynamically as a dimer-of-dimers.

The nature of the M2 molecular hinge motion is revealed particularly clearly if one analyses the principal motions in terms of kink and swivel angle. Thus, if we analyze the motions corresponding to the first two eigenvectors for a given M2 helix, there is a strong tendency for one component to correspond to a kink motion and one to a swivel. This is most evident for the octane simulations, again reflecting more extensive sampling. It should be noted that for some helices and simulations, the first eigenvector corresponds to kink and the second to swivel, whereas for other helices/simulations the order is reversed. However, the overall pattern is conserved. This is illustrated in Figure 5 for simulations OCT2 and PC3. From this analysis another pattern emerges: it can be seen that subunits 1 and 3 exhibit a different swivel angle from subunits 2 and 4. Thus, again a dimer-of-dimers type motion seems to emerge. However, this pattern is less evident in the POPC simulations, again possibly due to less extensive sampling.

Dimer-of-Dimers Motions of the M2 Helices. We have examined whether the dimer-of-dimers motions of the M2 helices seen in the KirBac1.1 and 3.1 simulations are associated with changes in the hydrophobic gate region that may be linked to (early events of) channel opening. Indeed, inspection of the time-dependent distances (Figure 6AC)

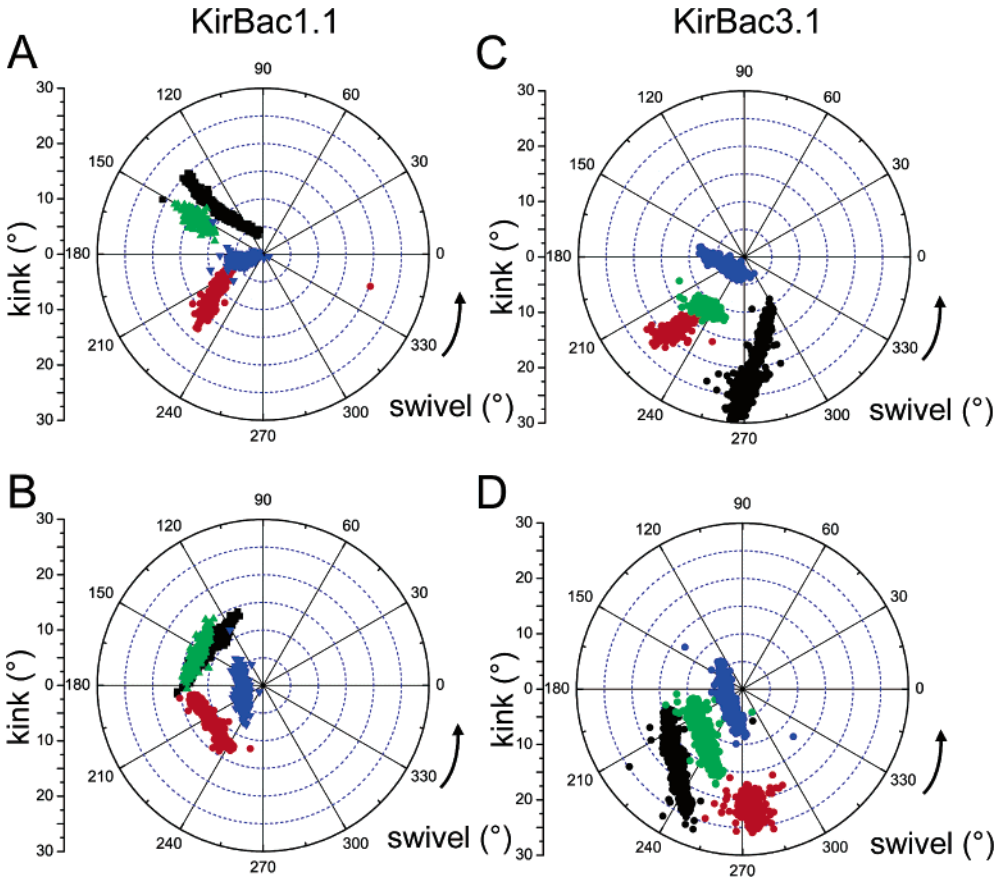

FIGURE 5: Analysis of kink and swivel angles of the M2 helices for simulations KirBac1.1 OCT2 and KirBac3.1 PC3 calculated after filtering the trajectories along selected principal components along eigenvectors 1 and 2. The eigenvectors have been sorted to show the predominant A, C kink and B, D swivel motions. The different colors correspond to different subunits, according to the following: black = monomer 1; red = monomer 2; green = monomer 3; blue = monomer 4.

between the Phe-146 (KirBac1.1) or Tyr-132 (KirBac3.1) residues supports the suggestion that dimer-of-dimers motions of the M2 helices are linked to changes in the conformation of the hydrophobic gate formed by this residue. In particular, in both simulations KirBac1.1 OCT1 and KirBac3.1 PC3 we observe a motion whereby two opposing M2 helices move apart while the other two opposing M2 helices move together. This perturbs the packing of the hydrophobic side chains in the intracellular gate region (Figure 6B).

DISCUSSION

In this study we have characterized the conformational dynamics of the inner (M2) helix bundle of KirBac1.1 and determined the dominant motions on a 20 ns time scale in terms of their kink and swivel angle components. The results of this analysis provide evidence in favor of a molecular hinge in the vicinity of Gly-134 (KirBac1.1) or Gly-120 (KirBac3.1). More detailed analysis of the motion in terms of kink and swivel angles suggest that the tetramer may behave as a dimer-of-dimers, with subunits 1 and 3, and subunits 2 and 4, moving together. This is consistent with the local 2-fold symmetry seen in the KirBac1.1 X-ray structure (*9*) and also with recent simulation studies on the isolated IC domains of mammalian Kir channels (*84*). More generally, simulation studies of the ligand-binding extracellular domain of the nicotinic acetylcholine receptor (*85*) have also revealed deviations from exact rotational symmetry.

The current results are consistent and reinforce previous computational studies aimed at exploring models of the open pore conformation of K channels. In particular, normal modes analysis (*22*), Monte Carlo methods (*52*), and nonequilibrium MD simulations (*86*) have all shown that an open pore conformation of KcsA can be achieved by the M2 helices kinking at a structural hinge located approximately at position Gly-99. This is consistent with crystallographic (*7*) and spectroscopic (*87*) data. For KirBac, our MD results indicate that the equivalent Gly provides a hinge point in both KirBac1.1 and 3.1. This is supported by modeling based on low resolution electron microscopy images (*53*). Thus, there appears to be a convergence of a number of approaches on a common model.

It is important to relate these simulation studies to experimental studies of K channel gating. There is a marked difference in conformation of M2 (or S6, its equivalent in Kv channels) between the X-ray structures of closed state K channels (namely KcsA, KirBac1.1, and KirBac3.1) and open state K channels (namely MthK, KvAP, and Kv1.2). This difference in conformation of M2 is very similar to that sampled in the simulations described in this paper (Figure 7). The molecular hinge corresponds to a conserved glycine residue (*7*) in the sequence of many K channels. In Kv channels the situation may be somewhat more complex, with a second hinge lower down the S6 helix associated with a conserved PVP sequence motif (*10*, *16*, *82*, *83*, *88*−*90*). In the case of Kv channels, mutations in the vicinity of both

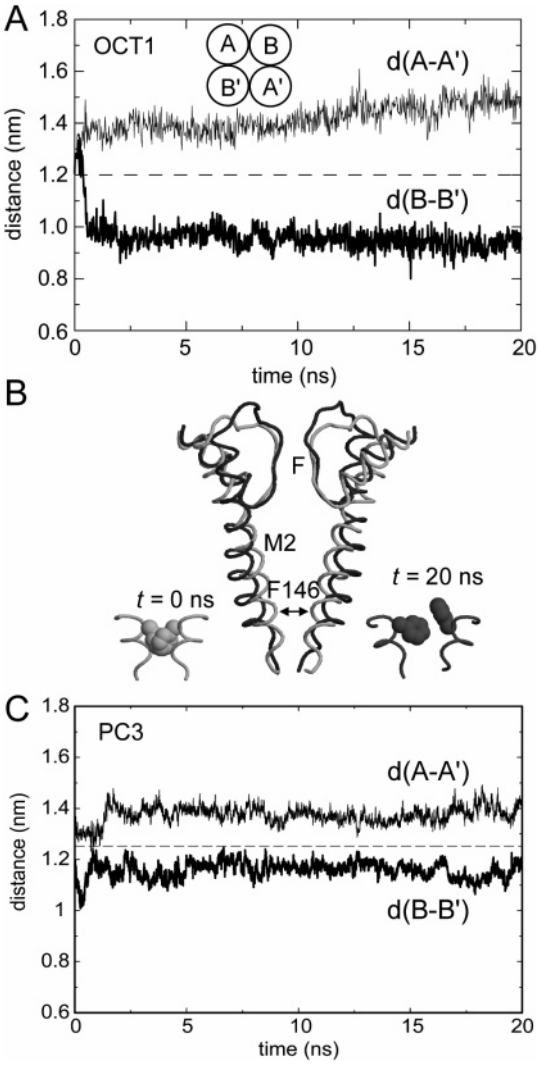

FIGURE 6: Dimer-of-dimers motions of the M2 helices as shown by monitoring the distance (A) between the Phe146 residues (backbone to backbone, where the distance is defined as from the center of mass of one group of N, Cα, and C atoms to the center of mass of the equivalent group in the opposite residue) as a function of time for opposite pairs of monomers (one pair, black line; the other pair, gray line) for KirBac1.1 simulation OCT1, or (C) between the Tyr-132 residues for KirBac3.1 simulation PC3. This analsysis suggests dimer-of-dimers motions of the M2 helices. (B) Snapshots from KirBac1.1 simulation OCT1 of the P-helix, filter, and M2 helices of two opposite monomers, at $t = 0$ (pale gray) and $t = 20$ ns (dark gray). The arrow indicates the Phe-146 distance, and the insets show the corresponding Phe-146 side chains.

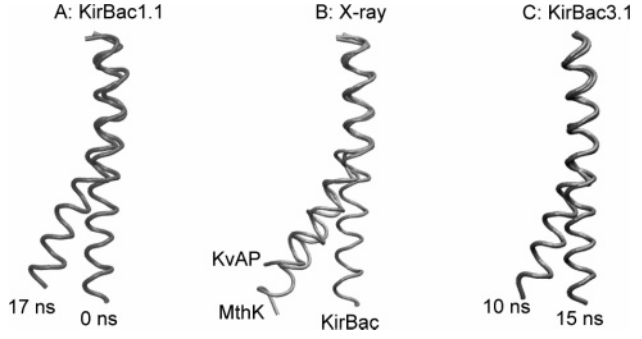

FIGURE 7: Comparison of MD and X-ray crystallographic results for kinking of M2. In A, selected structures of KirBac1.1 M2 helices from the start (0 ns) and toward the end (17 ns) of simulation OCT2 are shown. In B, the M2 helices from the crystal structures of KirBac (closed pore) and of MthK and KvAP (open pore) are shown. In C, selected structures of KirBac3.1 M2 helices from midway (~10 ns) and toward the end (15 ns) of simulation PC3 are shown. In all three diagrams, the N-terminal halves of the helices are used for fitting.

the conserved glycine hinge (*91*) and the second (PVP) hinge result in perturbations of channel gating (*92*−*94*). For Kir channels, proline scanning mutations combined with molecular modeling (*95*) support the suggested glycine molecular hinge. Comparable studies of the bacterial sodium channel NaChBac suggest a glycine hinge may also be present in the pore-lining helices of sodium channels (*96*). Unfortunately, such mutational data are as yet unavailable for KirBac1.1.

It is important to be aware of the limitations of the simulation approach used in the current study. In particular, we should stress again that a time scale of ~20 ns is insufficient to sample gating per se, which occurs on a 1 μs to 1 ms time scale. In an attempt to look beyond the time scale of the current (atomistic) simulations we have used a more coarse-grained approach, namely anisotropic network modeling (ANM). This approach has achieved some success in predicting larger scale conformational transitions of proteins (*72*, *73*). We have examined the predicted motions for the M2 helix bundle generated by an ANM calculation on the complete KirBac1.1 TM domain tetramer (Hall et al., manuscript in preparation). Significantly, a degree of helix bending about the center of the M2 helices is observed, in agreement with the atomistic simulations. There are, of course, some differences from the atomistic simulations. A limitation of current implementations of ANM is that sequence-specific aspects of protein mobility (e.g. glycine hinges in helices) are not (directly) incorporated.

A second limitation of the duration of current membrane protein simulations (~20 ns) is that it does not permit complete sampling of the motions that may be revealed by simulations (*78*). One way in which to improve the statistical significance of the motions observed in current simulations is to repeat the simulations for a related protein, which shares the same fold and function, which differs in sequence. In the current study we have used the recent KirBac3.1 structure for this purpose. It is encouraging that the M2 helix hinge motion and the resultant dimer-of-dimers motions of the M2 helices at the intracellular mouth seem to be conserved between the two KirBac channels.

While remaining aware of these limitations, we suggest that our results may enable us to capture some of the early stages of the gating process. The design of our simulations has been to maximize our sampling of M2 flexibility by (i) uncoupling the gate from the "gatekeeper" (i.e. simulating just the TM domain, without the regulatory IC domain) and (ii) comparing octane (lower viscosity) and POPC membrane simulations. Having revealed a possible dimer-of-dimers motion of the M2 helix hinges in the isolated TM domain of KirBac1.1, it will be important to analyze for similar motions in extended simulations of the intact KirBac channel (Domene et al., unpublished results) and of models (*97*) of mammalian Kir channels.

ACKNOWLEDGMENT

We thank our colleagues for their interest in and helpful comments on this work.

SUPPORTING INFORMATION AVAILABLE

Figure 8, showing the MSFs convergence analysis performed on the inner M2 helices bundle in all simulated systems. This material is available on the Internet free of charge at http://pubs.acs.org.

REFERENCES

1. Yellen, G. (2002) The voltage-gated potassium channels and their relatives, *Nature 419*, 35−42.
2. Mackinnon, R. (2003) Potassium channels, *FEBS Lett. 555*, 62−65.
3. Doyle, D. A., Cabral, J. M., Pfuetzner, R. A., Kuo, A., Gulbis, J. M., Cohen, S. L., Cahit, B. T., and MacKinnon, R. (1998) The structure of the potassium channel: molecular basis of K^+ conduction and selectivity, *Science 280*, 69−77.
4. Morais-Cabral, J. H., Zhou, Y., and MacKinnon, R. (2001) Energetic optimization of ion conduction by the K^+ selectvity filter, *Nature 414*, 37−42.
5. Zhou, Y., and MacKinnon, R. (2003) The occupancy of ions in the K^+ selectivity filter: charge balance and coupling of ion binding to a protein conformational change underlie high conduction rates, *J. Mol. Biol. 333*, 965−975.
6. Jiang, Y., Lee, A., Chen, J., Cadene, M., Chait, B. T., and MacKinnon, R. (2002) Crystal structure and mechanism of a calcium-gated potassium channel, *Nature 417*, 515−522.
7. Jiang, Y., Lee, A., Chen, J., Cadene, M., Chait, B. T., and MacKinnon, R. (2002) The open pore conformation of potassium channels, *Nature 417*, 523−526.
8. Jiang, Y., Lee, A., Chen, J., Ruta, V., Cadene, M., Chait, B. T., and Mackinnon, R. (2003) X-ray structure of a voltage-dependent K^+ channel, *Nature 423*, 33−41.
9. Kuo, A., Gulbis, J. M., Antcliff, J. F., Rahman, T., Lowe, E. D., Zimmer, J., Cuthbertson, J., Ashcroft, F. M., Ezaki, T., and Doyle, D. A. (2003) Crystal structure of the potassium channel KirBac1.1 in the closed state, *Science 300*, 1922−1926.
10. Long, S. B., Campbell, E. B., and MacKinnon, R. (2005) Crystal structure of a mammalian voltage-dependent *Shaker* family K^+ channel, *Science 309*, 897−902.
11. Nichols, C. G., and Lopatin, A. N. (1997) Inward rectifier potassium channels, *Annu. Rev. Physiol. 59*, 171−191.
12. Reimann, F., and Ashcroft, F. M. (1999) Inwardly rectifying potassium channels, *Curr. Opin. Cell Biol. 11*, 503−508.
13. Nishida, M., and MacKinnon, R. (2002) Structural basis of inward rectification: cytoplasmic pore of the G protein-gated inward rectifier GIRK1 at 1.8 Å resolution, *Cell 111*, 957−65.
14. Gulbis, J. M., Kuo, A., Smith, B., Doyle, D. A., Edwards, A., Arrowsmith, C., and Sundstrom, M. (2005) Two intermediate gating state crystal structures of the KirBac3.1 K^+ channel, manuscript in preparation.
15. Hille, B. (2001) *Ionic Channels of Excitable Membranes*, 3rd ed., Sinauer Associates Inc., Sunderland, Mass.
16. Webster, S. M., del Camino, D., Dekker, J. P., and Yellen, G. (2004) Intracellular gate opening in Shaker K^+ channels defined by high-affinity metal bridges, *Nature 428*, 864−868.
17. Du, X. O., Zhang, H. L., Lopes, C., Mirshahi, T., Rohacs, T., and Logothetis, D. E. (2004) Characteristic interactions with phosphatidylinositol 4,5-bisphosphate determine regulation of Kir channels by diverse modulators, *J. Biol. Chem. 279*, 37271−37281.
18. Dabrowski, M., Tarasov, A., and Ashcroft, F. M. (2004) Mapping the architecture of the ATP-binding site of the K-ATP channel subunit Kir6.2, *J. Physiol. 557*, 347−354.
19. Trapp, S., Haider, S., Sansom, M. S. P., Ashcroft, F. M., and Jones, P. (2003) Identification of residues contributing to the ATP binding site of Kir6.2, *EMBO J. 22*, 2903−2912.
20. Camino, D. D., Holmgren, M., Liu, Y., and Yellen, G. (2000) Blocker protection in the pore of a voltage-gated K^+ channel and its structural implications, *Nature 403*, 321−325.
21. Niu, X., Qian, X., and Magleby, K. L. (2004) Linker-gating ring complex as passive spring and Ca^{2+}-dependent machine for a voltage and Ca^{2+}-activated potassium channel, *Neuron 42*, 745−756.
22. Shen, Y. F., Kong, Y. F., and Ma, J. P. (2002) Intrinsic flexibility and gating mechanism of the potassium channel KcsA, *Proc. Natl. Acad. Sci. U.S.A. 99*, 1949−1953.
23. Biggin, P. C., Shrivastava, I. H., Smith, G. R., and Sansom, M. S. P. (2001) Nonequilibrium molecular dynamics study of KcsA gating, *Biophys. J. 80*, 514.
24. Holyoake, J., Domene, C., Bright, J. N., and Sansom, M. S. P. (2003) KcsA closed and open: modelling and simulation studies, *Eur. Biophys. J. 33*, 238−246.
25. Guidoni, L., Torre, V., and Carloni, P. (1999) Potassium and sodium binding in the outer mouth of the K^+ channel, *Biochemistry 38*, 8599−8604.
26. Guidoni, L., Torre, V., and Carloni, P. (2000) Water and potassium dynamics in the KcsA K^+ channel, *FEBS Lett. 477*, 37−42.
27. Åqvist, J., and Luzhkov, V. (2000) Ion permeation mechanism of the potassium channel, *Nature 404*, 881−884.
28. Luzhkov, V. B., and Åqvist, J. (2000) A computational study of ion binding and protonation states in the KcsA potassium channel *Biochim. Biophys. Acta 1481*, 360−370.
29. Shrivastava, I. H., and Sansom, M. S. P. (2000) Simulations of ion permeation through a potassium channel: molecular dynamics of KcsA in a phospholipid bilayer, *Biophys. J. 78*, 557−570.
30. Sansom, M. S. P., Shrivastava, I. H., Ranatunga, K. M., and Smith, G. R. (2000) Simulations of ion channels − watching ions and water move, *Trends Biochem. Sci. 25*, 368−374.
31. Jordan, P. (2000) in *Proceedins of the IMA Workshop on Membrane Transport and Renal Physiology* (Layton, H., Ed.), Springer-Verlag.
32. Bernèche, S., and Roux, B. (2000) Molecular dynamics of the KcsA K^+ channel in a bilayer membrane, *Biophys. J. 78*, 2900−2917.
33. Allen, T. W., Bliznyuk, A., Rendell, A. P., Kuyucak, S., and Chung, S. H. (2000) The potassium channel: structure, selectivity and diffusion, *J. Chem. Phys. 112*, 8191−8204.
34. Allen, T. W., and Chung, S. H. (2001) Brownian dynamics study of an open-state KcsA potassium channel, *Biochim. Biophys. Acta 1515*, 83−91.
35. Bernèche, S., and Roux, B. (2001) Energetics of ion conduction through the K^+ channel, *Nature 414*, 73−77.
36. Luzhkov, V. B., and Åqvist, J. (2001) Mechanisms of tetraethylammonium ion block in the KcsA potassium channel, *FEBS Lett. 495*, 191−196.
37. Mashl, R. J., Tang, Y. Z., Schnitzer, J., and Jakobsson, E. (2001) Hierarchical approach to predicting permeation in ion channels, *Biophys. J. 81*, 2473−2483.
38. Roux, B. (2002) Theoretical and computational models of ion channels, *Curr. Opin. Struct. Biol. 12*, 182−189.
39. Chung, S. H., and Kuyucak, S. (2002) Ion channels: recent progress and prospects, *Eur. Biophys. J. 31*, 283−293.
40. Guidoni, L., and Carloni, P. (2002) Potassium permeation through the KcsA channel: a density functional study, *Biochim. Biophys. Acta 1563*, 1−6.
41. Shrivastava, I. H., Tieleman, D. P., Biggin, P. C., and Sansom, M. S. P. (2002) K^+ vs. Na^+ ions in a K channel selectivity filter: a simulation study, *Biophys. J. 83*, 633−645.
42. Shrivastava, I. H., and Sansom, M. S. P. (2002) Molecular dynamics simulations and KcsA channel gating, *Eur. Biophys. J. 31*, 207−216.
43. Capener, C. E., and Sansom, M. S. P. (2002) MD Simulations of a K channel model − sensitivity to changes in ions, waters and membrane environment, *J. Phys. Chem. B 106*, 4543−4551.
44. Giorgetti, A., and Carloni, P. (2003) Molecular modeling of ion channels: structural predictions, *Curr. Opin. Chem. Biol. 7*, 150−156.
45. Domene, C., Bond, P., and Sansom, M. S. P. (2003) Membrane protein simulation: ion channels and bacterial outer membrane proteins, *Adv. Protein Chem. 66*, 159−193.
46. Berneche, S., and Roux, B. (2003) A microscopic view of ion conduction through the K^+ channel, *Proc. Natl. Acad. Sci. U.S.A. 100*, 8644−8648.
47. Noskov, S. Y., Bernèche, S., and Roux, B. (2004) Control of ion selectivity in potassium channels by electrostatic and dynamic properties of carbonyl ligands, *Nature 431*, 830−834.
48. Tikhonov, D. B., Mellor, I. R., and Usherwood, P. N. R. (2004) Modeling noncompetitive antagonism of a nicotinic acetylcholine receptor, *Biophys. J. 87*, 159−170.
49. Capener, C. E., Proks, P., Ashcroft, F. M., and Sansom, M. S. P. (2003) Filter flexibility in a mammalian K channel: models and simulations of Kir6.2 mutants, *Biophys. J. 84*, 2345−2356.
50. Allen, T. W., Andersen, O. S., and Roux, B. (2004) On the importance of atomic fluctuations, protein flexibility, and solvent in ion permeation, *J. Gen. Physiol. 124*, 679−690.

51. Domene, C., Grottesi, A., and Sansom, M. S. P. (2004) Filter flexibility and distortion in a bacterial inward rectifier K^+ channel: simulation studies of KirBac1.1, *Biophys. J. 87*, 256−267.
52. Tikhonov, D. B., and Zhorov, B. S. (2004) In silico activation of KcsA K+ channel by lateral forces applied to the C-termini of inner helices, *Biophys. J. 87*, 1526−1536.
53. Domene, C., Doyle, D. D., and Vénien-Bryan, C. (2005) Modeling of an ion channel in its open conformation, *Biophys. J. 89*, L101-L103.
54. Ranatunga, K. M., Shrivastava, I. H., Smith, G. R., and Sansom, M. S. P. (2001) Side-chain ionisation states in a potassium channel, *Biophys. J. 80*, 1210−1219.
55. Berendsen, H. J. C., Postma, J. P. M., van Gunsteren, W. F., and Hermans, J. (1981) *Intermolecular Forces*, Reidel, Dordrecht.
56. Domene, C., and Sansom, M. S. P. (2003) A potassium channel, ions and water: simulation studies based on the high-resolution X-ray structure of KcsA, *Biophys. J. 85*, 2787−2800.
57. Lindahl, E., Hess, B., and van der Spoel, D. (2001) GROMACS 3.0: a package for molecular simulation and trajectory analysis, *J. Mol. Model. 7*, 306−317.
58. van Gunsteren, W. F., and Berendsen, H. J. C. (1987) *Gromos-87 manual*, Biomos BV, Groningen.
59. Berger, O., Edholm, O., and Jahnig, F. (1997) Molecular dynamics simulations of a fluid bilayer of dipalmitoylphosphatidycholine at full hydration, constant pressure and constant temperature, *Biophys. J. 72*, 2002−2013.
60. Marrink, S. J., Berger, O., Tieleman, D. P., and Jahnig, F. (1998) Adhesion forces of lipids in a phospholipid membrane studied by molecular dynamics simulations, *Biophys. J. 74*, 931−943.
61. Åqvist, J. (1990) Ion water interaction potentials derived from free-energy perturbation simulations, *J. Phys. Chem. 94*, 8021−8024.
62. Hoover, W. G. (1985) Canonical dynamics: equilibrium phase-space distributions, *Phys. Rev. A31*, 1695−1697.
63. Darden, T., York, D., and Pedersen, L. (1993) Particle mesh Ewald − an N.log(N) method for Ewald sums in large systems, *J. Chem. Phys. 98*, 10089−10092.
64. Hess, B., Bekker, H., Berendsen, H. J. C., and Fraaije, J. G. E. M. (1997) LINCS: A linear constraint solver for molecular simulations, *J. Comput. Chem. 18*, 1463−1472.
65. Garcia, A. E. (1992) Large-amplitude nonlinear motions in proteins, *Phys. Rev. Lett. 68*, 2696−2699.
66. Amadei, A., Linssen, A. B. M., and Berendsen, H. J. C. (1993) Essential dynamics of proteins, *Proteins: Struct. Funct. Genet. 17*, 412−425.
67. Cordes, F. S., Bright, J. N., and Sansom, M. S. P. (2002) Proline-induced distortions of transmembrane helices, *J. Mol. Biol. 323*, 951−960.
68. Humphrey, W., Dalke, A., and Schulten, K. (1996) VMD − Visual Molecular Dynamics, *J. Mol. Graph. 14*, 33−38.
69. Sayle, R. A., and Milner-White, E. J. (1995) RasMol: Biomolecular graphics for all, *Trends Biochem. Sci. 20*, 374−376.
70. Hess, B. (2000) Similarities between principal components of protein dynamics and random diffusion, *Phys. Rev. E 62*, 8438−8448.
71. Hess, B. (2002) Convergence of sampling in protein simulations, *Phys. Rev. E 65*, art. no. 031910.
72. Keskin, O., Jernigan, R. L., and Bahar, I. (2000) Proteins with similar architecture exhibit similar large-scale dynamic behavior, *Biophys. J. 78*, 2093-2106.
73. Atilgan, A. R., Durell, S. R., Jernigan, R. L., Demirel, M. C., Keskin, O., and Bahar, I. (2001) Anisotropy of fluctuation dynamics of proteins with an elastic network model, *Biophys. J. 80*, 505−515.
74. Capener, C. E., Shrivastava, I. H., Ranatunga, K. M., Forrest, L. R., Smith, G. R., and Sansom, M. S. P. (2000) Homology modelling and molecular dynamics simulation studies of an inward rectifier potassium channel, *Biophys. J. 78*, 2929−2942.
75. Pang, A., Arinaminpathy, Y., Sansom, M. S. P., and Biggin, P. C. (2003) Interdomain dynamics and ligand binding: molecular dynamics simulations of glutamine binding protein, *FEBS Lett. 550*, 168−174.
76. Pang, A., Arinaminpathy, Y., Sansom, M. S. P., and Biggin, P. C. (2005) Comparative molecular dynamics − similar folds and similar motions? *Proteins: Struct. Funct. Bioinf.* (in press).
77. Bond, P. J., and Sansom, M. S. P. (2003) Membrane protein dynamics vs. environment: simulations of OmpA in a micelle and in a bilayer, *J. Mol. Biol. 329*, 1035−1053.
78. Faraldo-Gómez, J. D., Forrest, L. R., Baaden, M., Bond, P. J., Domene, C., Patargias, G., Cuthbertson, J., and Sansom, M. S. P. (2004) Conformational sampling and dynamics of membrane proteins from 10-nanosecond computer simulations, *Proteins: Struct. Funct. Bioinf. 57*, 783−791.
79. Amadei, A., Ceruso, M. A., and Di Nola, A. (1999) On the convergence of the conformational coordinates basis set obtained by the essential dynamics analysis of proteins' molecular dynamics simulations, *Proteins Struct. Funct. Genet. 36*, 419−424.
80. Ceruso, M. A., Grottesi, A., and Di Nola, A. (2003) Dynamic effects of mutations within two loops of cytochrome *c*(551) from *Pseudomonas aeruginosa Proteins Struct. Func. Genet. 50*, 222−229.
81. Bright, J. N., and Sansom, M. S. P. (2003) The flexing/twirling helix: exploring the flexibility about molecular hinges formed by proline and glycine motifs in transmembrane helices, *J. Phys. Chem. B 107*, 627−636.
82. Bright, J. N., Shrivastava, I. H., Cordes, F. S., and Sansom, M. S. P. (2002) Conformational dynamics of helix S6 from Shaker potassium channel: simulation studies, *Biopolymers 64*, 303−313.
83. Bright, J. N., and Sansom, M. S. P. (2004) The Kv channel S6 helix as a molecular switch: simulation studies, *IEE Proc.−Nanobiotechnol. 151*, 17−27.
84. Haider, S., Grottesi, A., Ashcroft, F. M., and Sansom, M. S. P. (2005) Conformational dynamics of the ligand-binding domain of inward rectifier K channels as revealed by MD simulations: towards an understanding of Kir channel gating *Biophys. J. 88*, 3310−3320.
85. Henchman, R. H., Wang, H. L., Sine, S. M., Taylor, P., and McCammon, J. A. (2003) Asymmetric structural motions of the homomeric α7 nicotinic receptor ligand binding domain revealed by molecular dynamics simulation, *Biophys. J. 85*, 3007−3018.
86. Biggin, P. C., and Sansom, M. S. P. (2002) Open-state models of a potassium channel, *Biophys. J. 83*, 1867−1876.
87. Liu, Y., Sompornpisut, P., and Perozo, E. (2001) Structure of the KcsA channel intracellular gate in the open state, *Nature Struct. Biol. 8*, 883−887.
88. Camino, D. D., and Yellen, G. (2001) Tight steric closure at the intracellular activation gate of a voltage-gated K^+ channel, *Neuron 32*, 649−656.
89. Beckstein, O., Biggin, P. C., Bond, P. J., Bright, J. N., Domene, C., Grottesi, A., Holyoake, J., and Sansom, M. S. P. (2003) Ion channel gating: insights via molecular simulations, *FEBS Lett. 555*, 85−90.
90. Long, S. B., Campbell, E. B., and MacKinnon, R. (2005) Voltage sensor of Kv1.2: structural basis of electromechanical coupling, *Science 309*, 903−908.
91. Magidovich, E., and Yifrach, O. (2004) Conserved gating hinge in ligand- and voltage-dependent K^+ channels, *Biochemistry 43*, 13242−13247.
92. Labro, A. J., Raes, A. L., Bellens, I., Ottschytsch, N., and Snyders, D. J. (2003) Gating of Shaker-type channels requires the flexibility of S6 caused by prolines, *J. Biol. Chem. 278*, 50724−50731.
93. Sukhareva, M., Hackos, D. H., and Swartz, K. (2003) Constitutive activation of the Shaker Kv channel, *J. Gen. Physiol. 122*, 541−556.
94. Hackos, D. H., Chang, T. H., and Swartz, K. J. (2002) Scanning the intracellular S6 activation gate in the shaker K+ channel, *J. Gen. Physiol. 119*, 521−531.
95. Jin, T., Peng, L., Mirshahi, T., Rohacs, T., Chan, K. W., Sanchez, R., and Logothetis, D. E. (2002) The $\beta\gamma$ subunits of G proteins gate a K+ channel by pivoted bending of a transmembrane segment, *Mol. Cell 10*, 469−481.
96. Zhao, Z., Yarov-Yarovoy, V., Scheuer, T., and Catterall, W. A. (2004) A gating hinge in Na^+ channels: a molecular switch for electrical signalling, *Neuron 41*, 859−865.
97. Antcliffe, J. F., Haider, S., Proks, P., Sansom, M. S. P., and Ashcroft, F. M. (2005) Functional analysis of a structural model of the ATP-binding site of the K_{ATP} channel Kir6.2 subunit, *EMBO J. 24*, 229−239.
98. Smart, O. S., Neduvelil, J. G., Wang, X., Wallace, B. A., and Sansom, M. S. P. (1996) Hole: A program for the analysis of the pore dimensions of ion channel structural models, *J. Mol. Graph. 14*, 354−360.

BI0510429